Int. J. Electrochem. Sci., 9 **(2014)** 1146 - 1162

International Journal of
ELECTROCHEMICAL
SCIENCE
www.electrochemsci.org

Review

Evaluation on the Efficiency of a Solar Powered Solid Oxide Electrolysis Cell Plant for Carbon Dioxide Reduction

Fangbing Wei[1], *Mingming Dao*[1], *Pengyu Song*[1], *Xiaomin Lu*[1], *Houcheng Zhang*[1,*], *Jinjie Zhang*[2,*], *Jinyong Zhu*[2], *Zuquan Zou*[3] , *Liwei Chen*[4]

[1] Department of Physics, Ningbo University, Ningbo 315211, China
[2] School of Marine Science, Ningbo University, Ningbo 315211, China
[3] Department of Preventive Medicine, Ningbo University, Ningbo 315211, China
[4] Mechanic and Electronic Engineering College, Sanming University, Sanming 365000, China
[*]E-mail: zhanghoucheng@nbu.edu.cn, zhangjinjie@nbu.edu.cn

Received: 28 October 2013 / *Accepted:* 4 December 2013 / *Published:* 5 January 2014

A new solid oxide electrolysis cell (SOEC) plant powered by solar energy for carbon dioxide reduction is established, in which the electrical/thermal energy production process, electrochemical reaction process, heat transfer processes, inlet gas compression process and products compression process are considered as the main energy consumption processes. The efficiency expressions for the plant are given under different operating conditions. Thermodynamic-electrochemical analysis shows that the joule heat generated from the irreversibilities in the SOEC may be larger than the thermal energy needed for the carbon dioxide reduction reaction. Some alternative plant layouts are designed to reasonably utilize the surplus waste heat in the SOEC, and accordingly, the expressions of the efficiency for the plant are modified. It is confirmed that the alternative plant layouts can effectively improve the performance of the plant. The effects of the support types of the SOEC, operating current density, operating temperature, operating pressure, effectiveness of heat exchangers and inlet flow rate of the carbon dioxide on the efficiency of the plant are revealed. The problem how to rationally operate the solar concentrating beam splitting subsystem to distribute the incident solar irradiance is solved.

Keywords: Solid oxide electrolysis cell; carbon dioxide reduction; solar energy; efficiency, exergy

1. INTRODUCTION

Conversion of CO_2 to valuable substance has become an important issue because increment of CO_2 level in the atmosphere leads to adverse impact on the environment [1]. CO_2 can be converted into formic acid, methane, ethane, ethylene, propylene, methanol and ethanol under different electrocatalytic conditions in different solvents [2-5]. There are many ways for conversion of

CO_2, including chemical, thermochemical, photochemical, biochemical, electrochemical and hydrothermal methods [6-9] . Among these, electrochemical method is an attractive technique due to its simple procedure and ambient operation conditions [10]. As one of the electrochemical approaches, the carbon dioxide can be electrolyzed into carbon monoxide and oxygen ($CO_2 \rightarrow CO+0.5\ O_2$) through solid oxide electrolysis cells (SOECs), where the produced carbon monoxide can be converted via Fischer Tropsch or methanation reactions to hydrocarbon fuels. NASA applied CO_2 electrolysis in SOECs as a mean for production over both platinum and nickel cermets electrodes [11-13]. Jensen et al. [14] showed the voltage-current density characteristics for CO_2 electrolysis in SOECs and the internal resistance was found to be 0.28 Ω at 1223 K. Ebbesen et al. [15] studied the carbon dioxide electrolysis in Ni/YSZ electrode supported SOECs consisting of a Ni-YSZ support, a Ni-YSZ electrode layer, a YSZ electrolyte and a LSM-YSZ O_2 electrode. It showed that long term CO_2 electrolysis was possible in SOECs with nickel electrodes.

As we know, the carbon dioxide splitting process is endothermic and it needs not only electrical energy but also thermal energy. A solar concentrating beam splitting system is a combination of photovoltaic (PV) and concentrating solar collector, which allows to produce both electricity and heat from one integrated system [16, 17]. With the rapid developments of the concentrating solar collectors, some scale up to 10 MW Dish concentrators with working temperature 1500-2000℃ have been already reported [18, 19]. The high operating temperature properties create an opportunity to combine the solar concentrating beam splitting subsystem with the SOEC subsystem for carbon dioxide reduction.

In this work, the concept of a solar powered SOEC plant for carbon dioxide electrochemical reduction is described, in which the main energy consumption processes in the plant are characterized and the expressions of the efficiency for the plant are specified under different operating conditions. Some alternatively plant layouts are designed to further utilize the waste heat produced in the SOEC and the corresponding efficiency expression will be modified. The effects of some microstructure parameters and operating conditions on the efficiency will be revealed. Finally, the problem how to rationally operate the solar concentrating beam splitting subsystem to distribute the incident solar irradiance is solved.

2. SOEC PLANT POWERED BY SOLAR ENERGY FOR CO_2 REDUCTION

2.1. Plant layout

Figure 1 shows the schematic diagram of a SOEC plant powered by solar energy for carbon dioxide reduction, which is adopted and modified from Refs. [20, 21]. The system is mainly composed of a solar concentrating beam splitting subsystem, a SOEC, two heat exchangers, a separator, three compressors, and two product tanks. The solar concentrating beam splitting subsystem converts the incident solar irradiance into electricity and heat. The generated electricity and heat are transferred to the SOEC to drive the carbon dioxide reduction reaction. As the products and remainders at the SOEC

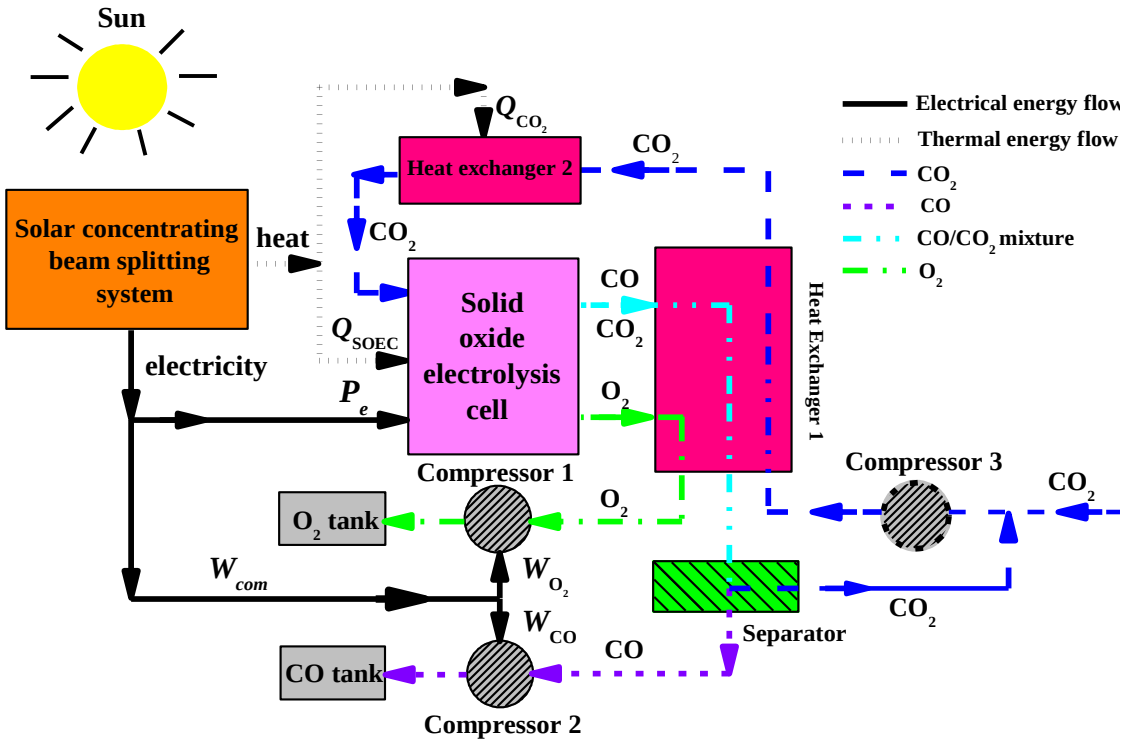

Figure 1. The schematic diagram of a solar powered SOEC plant for carbon dioxide reduction.

outlets contain a large fraction of the heat added to the feed CO_2, most part of the heat can be recovered by using a heat exchanger [22], such as heat exchanger 1 in Fig. 1. After leaving heat exchanger 1, oxygen gas is cooled down, compressed, and stored as by-product. Mixture CO/CO_2 flows into the separator and get separated, and then CO is cooled down, compressed, and stored as fuel. The hot CO_2 from the separator is mixed with the feeding CO_2 for the next CO_2 reduction cycle. Before reaching the desired operating conditions, the feeding CO_2 should be compressed by compressor 3 and further heated through heat exchanger 2. If the operating pressure of the SOEC equals to 1 atm, the compressor 3 in Fig. 1 can be saved.

2.2. Thermodynamic-electrochemical model of the SOEC

As shown in Fig. 1, the overall reaction of CO_2 reduction in a SOEC can be expressed as

$$CO_2 + \text{heat} + \text{electricity} \rightarrow CO + 0.5O_2 \quad (1)$$

The total theoretical energy demand for the above reaction, $\Delta H(T)$, is the sum of thermal energy demand $Q(T)$ and electrical energy demand $\Delta G(T)$ [23], i.e.,

$$\Delta H(T) = Q(T) + \Delta G(T), \quad (2)$$

where $Q(T) = T\Delta S(T)$, $\Delta S(T)$ is the change in the entropy, $\Delta G(T)$ is the change in the Gibbs free energy, T is the operating temperature of the SOEC. These thermodynamic parameters can be calculated by the thermophysical data provided in Ref. [23].

The reversible potential predicts the minimum electrical potential required to split CO_2 with a specific temperature and gas concentrations, which can be determined by the Nernst equation [23-25], i.e.,

$$E = E_0 + \frac{RT}{2F}\ln\left[\frac{P_{\mathrm{CO}}^0\left(P_{\mathrm{O}_2}^0\right)^{0.5}}{P_{\mathrm{CO}_2}^0}\right], \tag{3}$$

where $E_0 = \Delta G(T)/2F$ is the equilibrium potential at the standard pressure; R is the universal gas constant; F is the Faraday constant; and P_{CO}^0, $P_{\mathrm{CO}_2}^0$ and $P_{\mathrm{O}_2}^0$ are, respectively, the partial pressures of CO, CO_2, and O_2 at the electrode surfaces.

As previously described in Ref. [23], some irreversible losses are inevitable when the electrochemical reactions are proceeded in the SOEC, which primarily originate from the activation overpotential (V_{act}), concentratin overpotential (V_{con}), and ohmic overpotential (V_{ohm}). These overpotentials can be determined individually as follows:

$$V_{act,a} = \frac{RT}{F}\sinh^{-1}\left(\frac{J}{2J_{0,a}}\right) = \frac{RT}{F}\ln\left[\frac{J}{2J_{0,a}} + \sqrt{\left(\frac{J}{2J_{0,a}}\right)^2 + 1}\right], \tag{4}$$

$$V_{act,c} = \frac{RT}{F}\sinh^{-1}\left(\frac{J}{2J_{0,c}}\right) = \frac{RT}{F}\ln\left[\frac{J}{2J_{0,c}} + \sqrt{\left(\frac{J}{2J_{0,c}}\right)^2 + 1}\right], \tag{5}$$

$$V_{con,c} = \frac{RT}{2F}\left[\ln\left(1 + \frac{J}{J_{l\mathrm{CO}}}\right) - \ln\left(1 - \frac{J}{J_{l\mathrm{CO}_2}}\right)\right], \tag{6}$$

$$V_{con,a} = \frac{RT}{4F}\ln\left[\frac{\sqrt{\left(P_{\mathrm{O}_2}^0\right)^2 + JRT\mu L_a/(2FB_g)}}{P_{\mathrm{O}_2}^0}\right], \tag{7}$$

$$V_{ohm} = J\left(\frac{L_a}{\sigma_a} + \frac{L_c}{\sigma_c} + \frac{L_e}{\sigma_e}\right), \tag{8}$$

where J is the operating current density; $J_{0,k} = \gamma_k \exp[-E_{act,k}/(RT)]$ is the exchange current density ($k = a$ or c), subscripts a and c represent the anode and cathode, respectively; γ_k is the pre-exponential factor of the anode or cathode; $E_{act,k}$ is the activation energy level at the anode or cathode; $J_{l\mathrm{CO}} = 2FC_{\mathrm{CO}}^0 D_{\mathrm{CO}}^{eff}/(AL_c)$ and $J_{l\mathrm{CO}_2} = 2FC_{\mathrm{CO}_2}^0 D_{\mathrm{CO}_2}^{eff}/(AL_c)$ are the equivalent limiting current densities resulting from the mass transfer of CO and CO_2, respectively; C_{CO}^0 and $C_{\mathrm{CO}_2}^0$ are the gas concentrations of CO and CO_2 at the anode interface, respectively; D_{CO}^{eff} and $D_{\mathrm{CO}_2}^{eff}$ are the effective binary diffusion coefficients of CO and CO_2, respectively; μ is the dynamic viscosity of O_2; B_g is the flow permeability; L_a , L_c and L_e are, respectively, the thicknesses of the anode, cathode and electrolyte; σ_a , σ_c and σ_e are, respectively, the electrical or ionic conductivities of the anode, cathode and electrolyte. Zhang et al. [23] used the above electrochemical model to simulate the dependence of the cell potential on the operating current density for different inlet gas compositions, and found that the modeling results were in good agreement with the experimental data obtained by Ebbesen et al. [15].

To drive the carbon dioxide reduction reactions, the required voltage and electrical power of a single SOEC, are respectively, determined by

$$V = E + V_{act,a} + V_{act,c} + V_{con,a} + V_{con,c} + V_{ohm}, \quad (9)$$

and

$$P_e = VI, \quad (10)$$

where $I = JA$ is the electric current through the SOEC and A is the effective surface area of the SOEC. On the other hand, the overpotentials involved in the SOEC operation will result in joule heat flow generation Q_J,

$$Q_J = (V_{act,a} + V_{act,c} + V_{con,a} + V_{con,c} + V_{ohm})I, \quad (11)$$

this amount of heat flow can be directly transferred to the carbon dioxide reduction reaction, and thus, the amount of heat supplied from solar concentrating beam splitting subsystem can be reduced from Q_1 ($= IT\Delta S / 2F$) to [20]

$$Q_{SOEC} = Q_1 - Q_J. \quad (12)$$

If $Q_{SOEC} \le 0$, it means that the joule heat generated from irreversible losses is equal to or larger than the theoretical heat required for the carbon dioxide reduction reaction. In this case, no external heat is necessary to provide to the SOEC and the surplus heat should be immediately removed to the environment via radiation and/or convection to ensure the SOEC's normal operation.

2.3. Heat exchangers and compressors

The exchanger 1 in Fig. 1 absorbers the heat contained in the products/ remainders and preheats the inlet CO_2 to attain a certain temperature, and the inlet CO_2 will be further heated by the solar concentrating beam splitting subsystem through heat exchanger 2 to reach the operating temperature of the SOEC. The heat flow required for heating the inlet CO_2, Q_{CO_2}, is given by [22]

$$Q_{CO_2} = [N_{CO_2,in}(\frac{1}{\varepsilon} - 1) + N_{CO_2,reacted}]\int_{T_0}^{T} C_{p,CO_2} dT - N_{CO,out}\int_{T_0}^{T} C_{p,CO} dT - N_{O_2,out}\int_{T_0}^{T} C_{p,O_2} dT, \quad (13)$$

where $N_{CO_2,in}$ is the inlet flow rate of CO_2, $N_{CO_2,reacted} = I/(2F)$ is the consumption rate of CO_2, $N_{CO,out} = I/(2F)$ and $N_{O_2,out} = I/(4F)$ are the outlet flow rates of the CO and O_2, respectively [20, 23], ε is the effectiveness of the heat exchangers, $C_{p,m}$ (m = CO_2, CO, or O_2) are the molar heat capacities of reactant/products, T_0 is the temperature of the environment.

In order to reduce the storage volume of the products, gas compressors are usually employed to compress the products, and the electric power consumed is given by [26, 27]

$$W_{com} = W_{O_2} + W_{CO} = C_{p,O_2} N_{O_2,out} \frac{T_0}{\eta_{com1}}\left[\left(P_{r,O_2}\right)^{\gamma-1/\gamma} - 1\right] + C_{p,CO} N_{CO,out} \frac{T_0}{\eta_{com2}}\left[\left(P_{r,CO}\right)^{\gamma-1/\gamma} - 1\right], \quad (14)$$

where η_{comp1} and η_{comp2} are, respectively, the efficiencies of compressor 1 and compressor 2; γ is the specific heat ratio; P_{r,O_2} and $P_{r,CO}$ are, respectively, the compression ratios of O_2 and CO after and before compressed.

If the operating pressure of the SOEC, P, is larger than 1 atm, compressor 3 in Fig. 1 should be put into operation and the amount of electrical power cost to compress the inlet CO_2 is given by [26, 27]

$$W_{\mathrm{CO}_2} = C_{\mathrm{p,\,CO}_2} N_{\mathrm{CO}_2,in} \frac{T_0}{\eta_{com3}} \left[\left(P_{r,\mathrm{CO}_2} \right)^{\gamma\text{-}1/\gamma} - 1 \right], \quad (15)$$

where η_{comp3} is the efficiency of compressor 3, P_{r,CO_2} is the ratio between the operating pressure of the SOEC and the ambient pressure.

2.4. Efficiency expressions of the plant

The efficiency of the system can be evaluated in terms of energy efficiency or exergy efficiency [20, 28]. Compared with the energy efficiency, the exergy efficiency provides more useful information which can directly impact process designs and improvements because exergy methods help in understanding and improving efficiency, environmental and economic performance as well as sustainability [29]. Thus, the exergy efficiency is adopted in evaluating the performance of the plant here. The overall exergy efficiency of the solar-driven SOEC CO_2 reduction plant, η, is equal to the product of the exergy efficiency of the solar concentrating beam splitting subsystem, η_s, and the exergy efficiency of the SOEC carbon dioxide reduction subsystem, η_c, i.e.,

$$\eta = \eta_s \eta_c . \quad (16)$$

The exergy efficiency of the solar concentrating beam splitting subsystem can be defined as [30, 31]

$$\eta_s = \frac{E_x}{E_{x,\mathrm{solar}}} = \frac{I_m V_m + F_R A_A [\rho_R \alpha_A (C A_A I_S - I_m V_m)/A_A - U_L (T_s - T_0) - \tau\sigma (T_s^4 - T_0^4)](1 - T_0/T_s)}{I_s C A_A (1 - T_0/T_{sun})} \quad (17)$$

where E_x is the output exergy from the solar concentrating beam splitting system; $E_{x,\mathrm{solar}}$ is the total exergy from the incident solar irradiance; I_m and V_m are the voltage and electrical current generated by the PV; F_R is the heat removal factor of the collector; A_A is the area of the absorber surface; C is the concentration ratio of the concentrating solar collector; σ is the Stefan's constant; ρ_R, α_A and τ are the reflectivity, absorptivity and emissivity of the collector, respectively; I_S is the solar intensity; U_L is the convection heat loss coefficient; T_s is the outlet temperature of the heat from the solar collector; T_{sun} is the temperature of the sun. The existing literatures have shown that the exergy efficiency of a hybrid photovoltaic/thermal (PV/T) system is in the ranges of 10.31-15% [31-33], the main exergy destruction of a solar powered SOEC plant for carbon dioxide reduction happens in the process of converting incident solar irradiance to electrical/thermal energy. For conservative consideration, the exergy efficiency of the solar concentrating beam splitting subsystem is set to 10% as not only the convection heat losses but also the radiation heat losses from the high temperature concentrating solar collector should be taken into account [31, 34].

The exergy efficiency of the SOEC carbon dioxide reduction subsystem can be expressed as [20]

$$\eta_c = \frac{N_{CO,out}E_{CO}}{P_e + W_{com} + Q_{SOEC}(1-\frac{T_0}{T_x}) + Q_{CO_2}(1-\frac{T_0}{T_s})} \quad (P=1 \text{ atm}) \quad (18)$$

or

$$\eta_c = \frac{N_{CO,out}E_{CO}}{P_e + W_{com} + W_{CO_2} + Q_{SOEC}(1-\frac{T_0}{T_x}) + Q_{CO_2}(1-\frac{T_0}{T_s})} \quad (P>1 \text{ atm}) \quad (19)$$

where E_{CO} is the exergy content of CO, the value of T_x may be equal to T_s, T or T_0, which depends on not only the sign of Q_{SOEC} but also the layout of the plant.

The exergy of a substance contains four parts, namely, physical exergy, kinetic exergy, potential exergy, and chemical exergy. Neglecting the small kinetic and potential exergies [35], the exergy content of CO is the sum of the physical exergy and the chemical exergy, i.e.,

$$E_{CO} = E_{CO,chem} + E_{CO,phys}, \quad (20)$$

where the value of $E_{CO,chem}$ can be directly found in Ref. [36], and the physical exergy of CO can be determined by using the following expression:

$$E_{CO,phys} = (h - h_o) - T_0(s - s_0) \quad (21)$$

where *h* and *s* represent the molar enthalpy and molar entropy of CO respectively, the subscript 0 denotes the reference environment condition.

3. DISCUSSION

It is clearly seen from Equations (2)-(21) that the exergy efficiency of the solar-driven SOEC carbon dioxide reduction plant depends on a set of designing and operating parameters such as the geometric parameters of the solar concentrating beam splitting subsystem, the microstructure parameters of an SOEC, operating temperature, operating pressure, operating current density, and efficiency of the compressors. In the following, parametric studies are carried out based on the parameters summarized in Tables 1 [20, 23, 36], and these parameters are kept constant unless specifically mentioned. Figure 2 shows that the thermal energy required for a SOEC per unit time, Q_{SOEC}, first increases from zero and then decreases to below zero as the current density is increased, and there exists a critical current density J_c corresponding to $Q_{SOEC} = 0$. Q_{SOEC} increases as the operating temperature is increased and the value of J_c shifts to a larger one as the operating temperature is increased.

When $0 < J \le J_c$ ($Q_{SOEC} \ge 0$), the amount of heat from the solar concentrating beam splitting subsystem, Q_{SOEC}, should be supplied to the SOEC to make it normally work, and the exergy content of the heat provided to the SOEC carbon dioxide reduction subsystem is determined by $Q_T = Q_{SOEC}(1-T_0/T_s) + Q_{CO_2}(1-T_0/T_s)$. For this case, η_c can be expressed by substituting $T_s = T_x$ into Eq. (18) or Eq. (19).

Table 1. Parameters used in the modeling [20, 23, 24, 36].

Parameter	Value
Charge transfer coefficient, α	0.5
Faraday constant, F (C mol^{-1})	96485
Universal gas constant, R (J mol^{-1} K^{-1})	8.314
Operating pressure, P (atm)	1.0
Pre-exponential factor, γ_a (A m^{-2})	2.051×10^{9} [23]
Pre-exponential factor, γ_c (A m^{-2})	1.344×10^{10} [23]
Activation energy for anode, E_{acta} (J mol^{-1})	1.2×10^{5} [23]
Activation energy for cathode, E_{actc} (J mol^{-1})	1.0×10^{5} [23]
Electrode porosity, ω (%)	40 [24]
Electrode tortuosity,ξ	5.0 [24]
Average pore radius, r (m)	0.5×10^{-6} [24]
Anode thickness, L_a (m)	5.0×10^{-4}[24]
Anode electric conductivity, σ_a (Ω^{-1} m^{-1})	8.4×10^{3} [23]
Cathode thickness , L_c (m)	5.0×10^{-5}[24]
Cathode electric conductivity, σ_c (Ω^{-1} m^{-1})	8.0×10^{4} [23]
Electrolyte thickness , L_e (m)	5.0×10^{-5} [24]
Electrolyte ionic conductivity, σ_e (Ω^{-1} m^{-1})	$3.34\times10^{4}\exp(-1.03\times10^{4}/T)$ [23]
Diameters of the CO molecular collision, σ_{CO} (Å)	3.690 [23,24]
Diameters of the CO_2 molecular collision,σ_{CO2} (Å)	3.941 [23,24]
Effective surface area of an SOEC, A (m^2)	6.4×10^{-3} [23]
Cathode interface gas compositions	70 mol% CO_2/30 mol%CO
Compression ratios of CO and O_2, $P_{r,CO}=P_{r,O2}$	50
Isentropic compression ratio, γ	1.4
Efficiencies of compressors, $\eta_{comp1}=\eta_{comp2}=\eta_{comp3}$	80%
Effectiveness of the heat exchangers, ε	0.8 [20]
Exergy efficiency of the solar concentrating beam splitting subsystem, η_s	10%
Flow rate of CO_2 at SOEC inlet, $N_{H2O,in}$ (mol s^{-1})	1.0×10^{-3}
Chemical exergy of CO, $E_{CO,chem}$ (J/mol)	2.7543×10^{5} [36]
Temperature of the SOEC, T (K)	1073
Temperature of the heat from concentrating collector , T_s (K)	1300
Temperature of environment, T_0 (K)	298

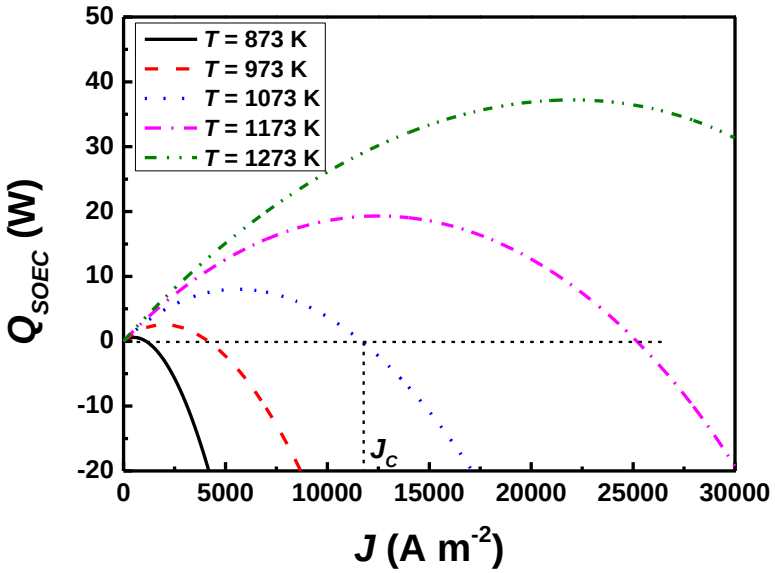

Figure 2. The curves of Q_{SOEC} varying with the current density for different operating temperatures, where J_c is the current density corresponding to $Q_{SOEC}=0$.

When $J > J_c$ ($Q_{SOEC} < 0$), the joule heat generated from the irreversibilities is larger than the thermal energy demand for the carbon dioxide reduction processes, no thermal energy from the solar concentrating beam splitting subsystem is necessary to provide to the SOEC and there exist some surplus joule heat. If the surplus joule heat is directly released to the environment without any utilization, as shown in Fig. 4 (a), the exergy content of the heat provided to the SOEC is equal to $Q_{CO_2}(1-T_0/T_s)$. For this case, the plant configuration is simple and η_c can be described by substituting $T_0 = T_x$ into Eq. (18) or Eq. (19).

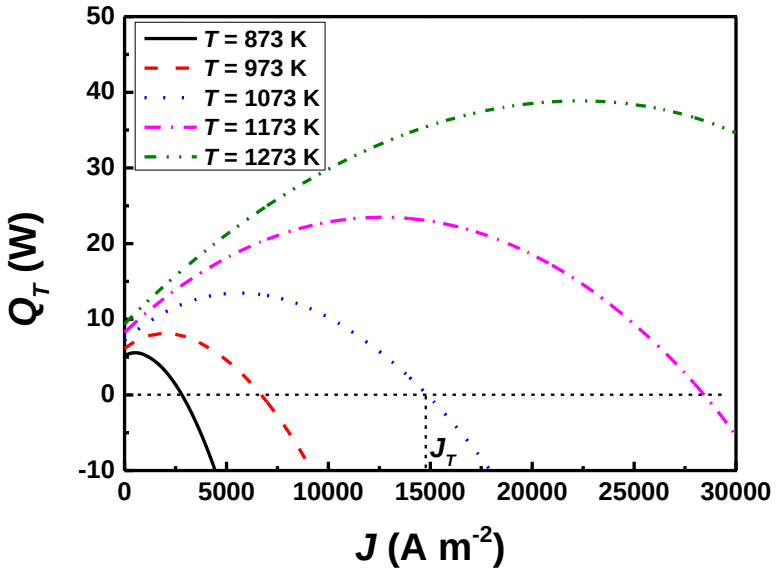

Figure 3. The curves of Q_T varying with the current density for different operating temperatures, where J_T is the operating current density corresponding to $Q_T = 0$.

As an alternative, when $J > J_c$ ($Q_{SOEC} < 0$), the surplus joule heat, Q_{SOEC}, can be transferred to heat the inlet CO_2 such that the thermal energy from the solar concentrating beam splitting subsystem can be reduced and more solar irradiance can be converted into electricity for SOEC, and η_c cannot be described by Eqs. (18) and (19) any more. In order to quantitatively explain this problem, one may define the algebraic sum of the exergy content of Q_{SOEC} and the exergy content of Q_{CO_2} as $Q_T = Q_{SOEC}(1-T_0/T) + Q_{CO_2}(1-T_0/T_s)$, the curves of Q_T varying with the operating current density for different operating temperature are shown in Fig. 3. It is seen from Fig. 3 that Q_T first increases from zero and then decreases to below zero as the current density is increased, obviously, the critical current density at $Q_T = 0$, J_T, is larger than J_c, and $Q_T > 0$ in the region of $J < J_T$ and $Q_T \le 0$ in the region of $J \ge J_T$.

When $J < J_T$, the redundant heat $|Q_{SOEC}|$ generated in the SOEC may be transferred to heat the inlet CO_2 through heat exchanger 2, thus the amount of heat from the solar concentrating beam splitting subsystem can be reduced from Q_{CO_2} to $\left[Q_{CO_2} - |Q_{SOEC}|(1-T_0/T)T_s/(T_s-T_0)\right]$ as shown in Fig. 4 (b), where $\left[|Q_{SOEC}|(1-T_0/T)T_s/(T_s-T_0)\right]$ is the equivalent amount of $|Q_{SOEC}|$ provided at

temperature T_s [22]. The exergy content of the heat provided to the SOEC can be reduced from $Q_{CO_2}(1-T_0/T_s)$ to $\left[Q_{CO_2}(1-T_0/T_s)-|Q_{SOEC}|(1-T_0/T)\right]$. For this case, η_c should be modified to

$$\eta_c = \frac{N_{CO,out}E_{CO}}{P_e + W_{com} + Q_{CO_2}\left(1-\frac{T_0}{T_s}\right) - |Q_{SOEC}|\left(1-\frac{T_0}{T}\right)} \qquad (P=1 \text{ atm}) \qquad (18a)$$

or

$$\eta_c = \frac{N_{CO,out}E_{CO}}{P_e + W_{com} + W_{CO_2} + Q_{CO_2}\left(1-\frac{T_0}{T_s}\right) - |Q_{SOEC}|\left(1-\frac{T_0}{T}\right)} \qquad (P>1 \text{ atm}) \qquad (19a)$$

When $J \geq J_T$, the amount of the redundant heat $|Q_{SOEC}|$ is so large that the heat Q_{CO_2} supplied by the solar concentrating beam splitting subsystem can be saved and all incident solar irradiance should be converted into electricity for SOEC, as shown in Fig. 4 (c).

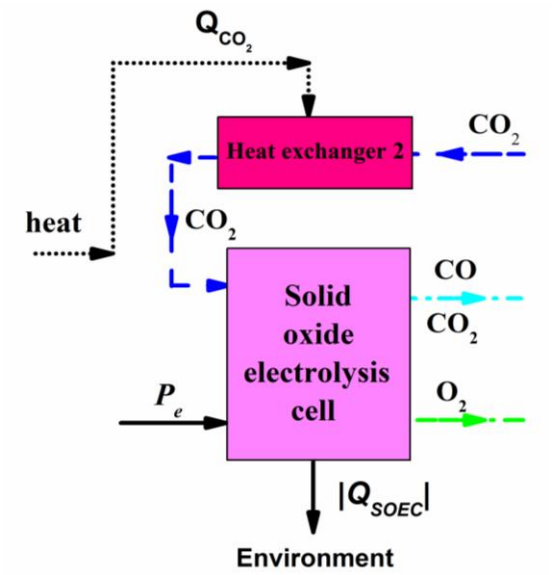

(a)

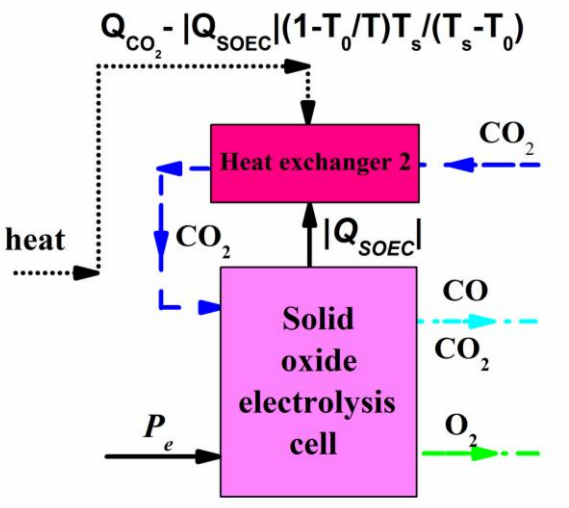

(b)

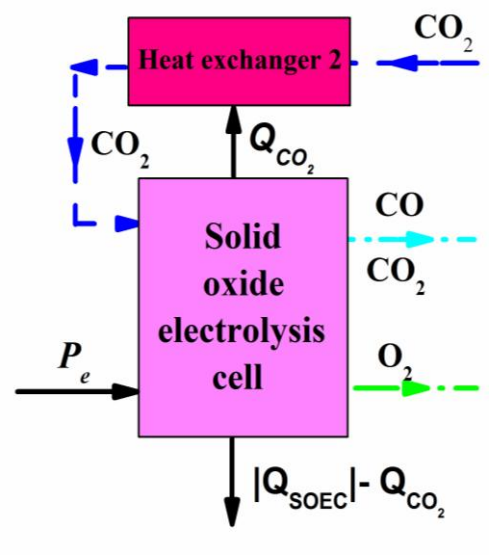

(c)

Figure 4. The part schematic diagram of a solar powered SOEC plant for carbon dioxide reduction, the rest part is the same as Fig. 1. (a) $|Q_{SOEC}|$ is directly released to the environment without any utilization, (b) $|Q_{SOEC}|$ is fully utilized ($J \le J_T$), and (c) $|Q_{SOEC}|$ is partly utilized ($J > J_T$).

The amount of heat transferred from the SOEC to heat exchanger 2 at temperature T, Q_{CO_2}, is equivalent to $|Q_{SOEC}|(1-T_0/T)T_s/(T_s-T_0)$ at temperature T_s, and the amount of the redundant heat released to the environment is equal to $|Q_{SOEC}|[1-(1-T_0/T)T_s/(T_s-T_0)]$ [22]. In such a case, η_c should be modified to

$$\eta_c = \frac{N_{CO,out}E_{CO}}{P_e + W_{com}} \qquad (P = 1 \text{ atm}) \qquad (18b)$$

or

$$\eta_c = \frac{N_{CO,out}E_{CO}}{P_e + W_{com} + W_{CO_2}} \qquad (P > 1 \text{ atm}) \qquad (19b)$$

It is seen from Fig. 5 that the alternative plant layouts in Fig. 4 show their advantages when the operating current density is larger than J_c, especially in the region of $J_c < J < J_T$. The efficiency first increases and then decreases as the operating current density is increased, and there exists a maximum efficiency $\eta_{\max}$. Both the maximum efficiency $\eta_{\max}$ and the current density corresponding to the maximum efficiency J_{m} increase monotonically with the increasing of the operating temperature. It is also shown in Fig. 5 that the efficiency of the system increases as the operating temperature is increased because the higher operating temperature will lessen the cathodic and anodic overpotentials and promote the electrode activity.

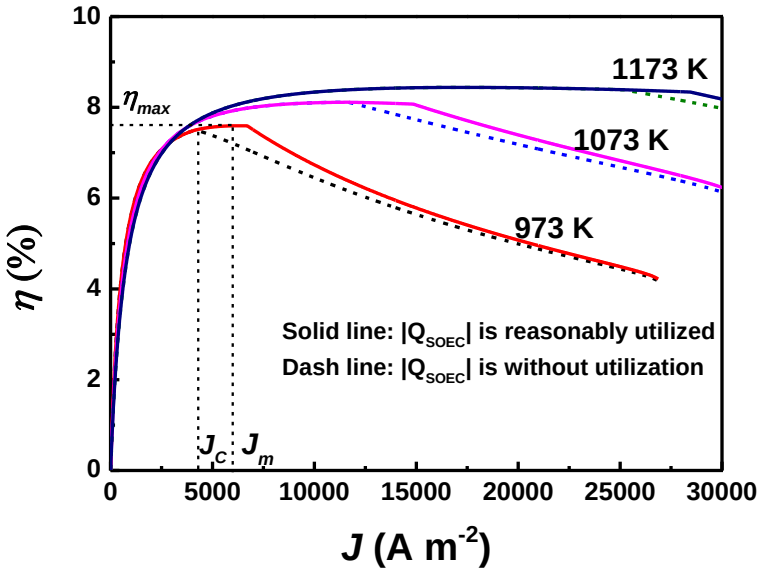

Figure 5. The curves of the efficiency varying with the current density for different temperature and different plant layouts, where the dash lines represent the waste heat $|Q_{SOEC}|$ are without any utilization, the solid lines represent the waste heat $|Q_{SOEC}|$ are utilized through the plant layout shown in Fig. 4.

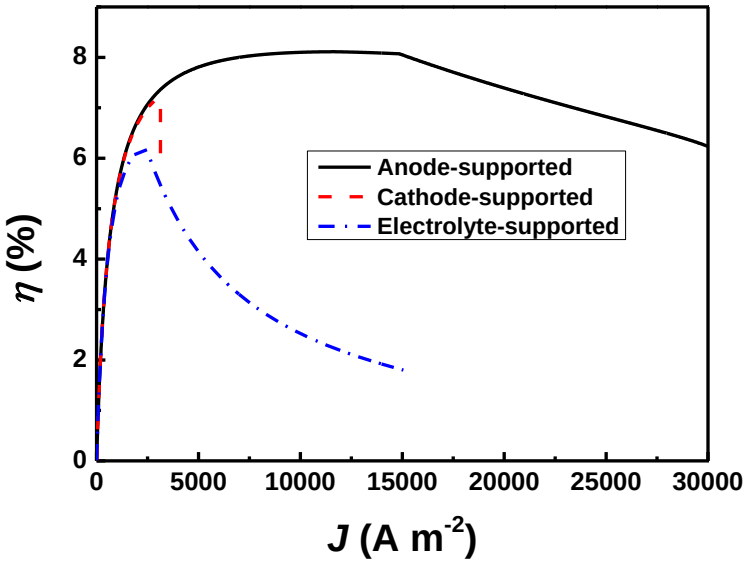

Figure 6. The $\eta - J$ characteristics of the SOEC with different supports types, where the thicknesses of the anode, cathode, and electrolyte of an anode-supported SOEC are 500 μm, 50 μm, and 50 μm, the component thicknesses of a cathode-supported type are 50 μm, 500 μm, and 50 μm, and the component thicknesses of an electrolyte-supported type are 100 μm, 100 μm, and 1000 μm in sequence [37], respectively.

The curves of $\eta - J$ with different support types of the SOEC are shown in Fig. 6. It is seen from Fig. 6 that the efficiency of the electrolyte-supported SOEC plant is the smallest among the three

types. The efficiency of the cathode-supported SOEC plant is larger than that of the electrolyte-supported one, but it will quickly decrease after it attains the maximum because the cathode concentration overpotential increases very quickly when the operating current density approaches the limiting current density. As shown in Fig. 6, this limiting current density is found to be about 3140 A m^{-2}, the comparative small limiting current density will restrict the achievement of higher reaction rate. The anode-supported SOEC shows the highest efficiency as the transport of the reactant (O^{2-}) in the anode is not limited by the porous structure, and there is no limiting current density even for a thick anode. Thus, the anode-supported SOEC is chosen as the most favorable design in the present paper.

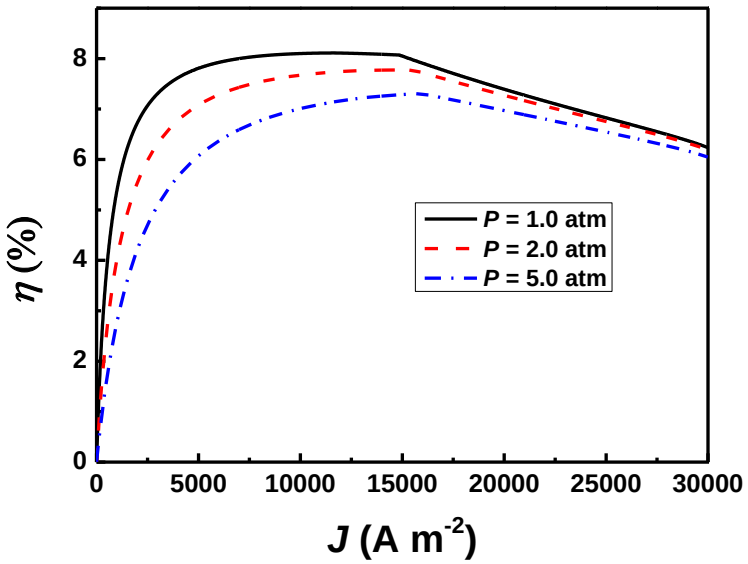

Figure 7. The effects of the operating pressure on the $\eta - J$ characteristics.

The effects of the operating pressure on the $\eta - J$ characteristics are shown in Fig. 7. It is seen from Fig. 7 that the effects of the operating pressure on the efficiency of the plant are less significant in the two extremes of the operating current density. Although the higher operating pressure may reduce the input voltage of the SOEC [23], the higher operating pressure also leads to more electrical energy consumption in the inlet gas compression process. As the electrical energy saved due to the higher operating pressure is smaller than that cost in the inlet gas compression process, the larger operating pressure will result in a reduction in the efficiency of the plant. However, higher operating pressure is more favorable in the practice because it will increase the reaction rate and thus increase the CO production rate.

The influence of the effectiveness of the heat exchangers on the efficiency of the plant is shown in Fig. 8. The efficiency increases as the effectiveness of the heat exchangers is increased, however, this influence only happens in the region of $J \le J_T$. When $J > J_T$, the redundant heat $|Q_{SOEC}|$ is so large that no more thermal energy is required and the influence of the effectiveness of the heat exchangers can be neglected. The influence of the inlet flow rate of carbon dioxide on the efficiency of the system is shown in Fig. 9. It shows that the efficiency of the system increases as the inlet flow rate

of carbon dioxide is decreased. Similarly, this influence mainly happens in the region of $J \le J_T$ and the influence can be negligible in the region of $J > J_T$.

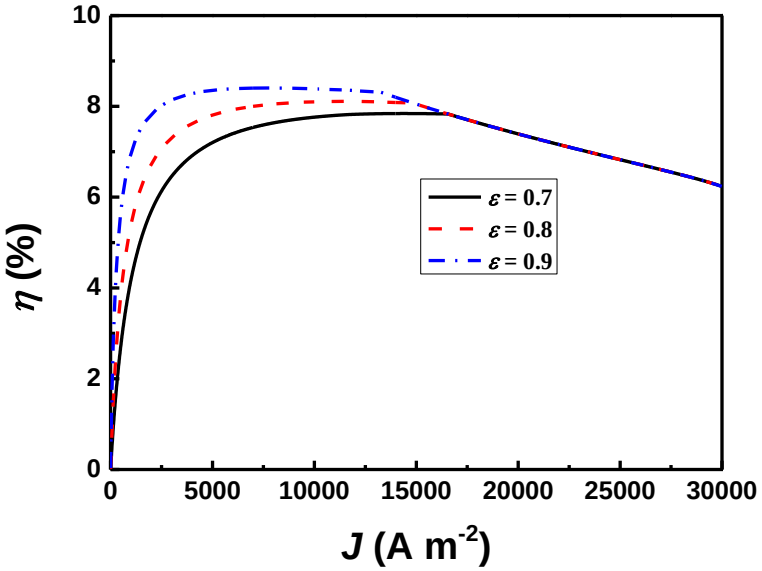

Figure 8. The effects of the effectiveness of the heat exchangers on the $\eta - J$ characteristics.

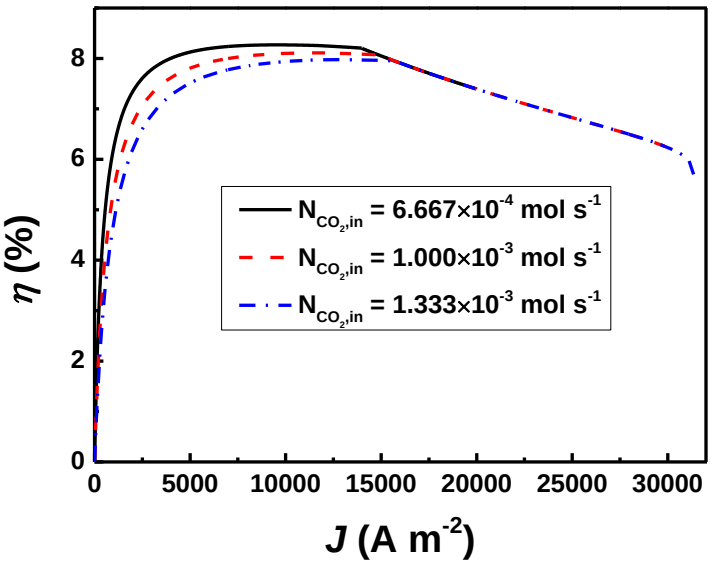

Figure 9. The effects of the inlet flow rate of carbon dioxide on the $\eta - J$ characteristics.

How to rationally split the inlet solar irradiance for electricity generation or for thermal energy production is essential for the performance improvement of the plant. For this purpose, one may introduce a balance parameter defined as the ratio of the required electrical energy to the total input exergy of the SOEC subsystem [21], i.e.,

$$\chi = \frac{P_e + W_{com}}{E_T} = \frac{P_e + W_{com}}{P_e + W_{com} + Q_{SOSE}(1 - \frac{T_0}{T_x}) + Q_{H_2O}(1 - \frac{T_0}{T_s})} \quad (P = 1 \text{ atm}) \quad (22)$$

or

$$\chi = \frac{P_e + W_{com} + W_{CO_2}}{E_T} = \frac{P_e + W_{com} + W_{CO_2}}{P_e + W_{com} + W_{CO_2} + Q_{SOSE}(1 - \frac{T_0}{T_x}) + Q_{H_2O}(1 - \frac{T_0}{T_s})}, \quad (P > 1 \text{ atm}) \quad (23)$$

to control the operation of the solar concentrating beam splitting subsystem, where E_T is the total exergy requirement of the SOEC subsystem.

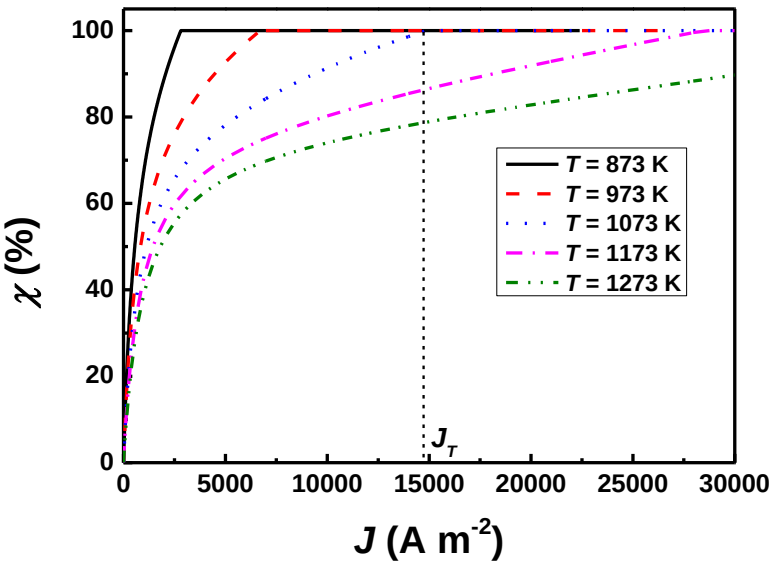

Figure 10. The curves of the balance parameter varying with the operating current density for different temperatures.

Figure 10 shows the curves of the balance parameter varying with the operating current density for different temperatures. When $J < J_T$, the balance parameter increases with the decreasing operating temperature or increasing operating current density, and the solar concentrating beam splitting subsystem should be operated as a so-called PV/T mode described in Ref. [38, 39]. When $J \geq J_T$, the balance parameter attains 100% and then keeps constant, and the solar concentrating beam splitting subsystem should be operated in the photovoltaic mode.

4. CONCLUSIONS

The concept of carbon dioxide electrochemical reduction through SOEC powered by solar energy is demonstrated in the present paper, the expressions for the efficiency of the plant are given by considering the main energy consumption processes such as the electrical/thermal energy production process, electrochemical reaction process, heat transfer process, inlet gas compression process and

product compression process. It is pointed out that the expressions are closely associated with the operating conditions and the waste heat recovery strategies. In order to effectively utilize the surplus waste heat in the SOEC, some alternative plant layouts are presented and the corresponding expressions of efficiency are also modified. It shows that the alternative plant layouts can effectively improve the efficiency of the system. The effects of some SOEC microstructure parameter and operating conditions such as dimension of SOEC components, operating temperature, operating pressure, effectiveness of heat exchangers and carbon dioxide inlet rate are also discussed. Finally, the problem how to rationally operate the solar concentrating beam splitting subsystem to convert the incident solar irradiance for electrical energy or for thermal energy is clearly articulated.

ACKNOWLEDGMENTS
This work has been supported by K. C. Wong Magna Fund in Ningbo University, Foundations of Zhejiang Educational Commission (No. Y201326937, No. Y200908119, and No. Y201327177), Natural Science Foundations of Ningbo City (No. 2013A610139, No. 2010A610057, and No. 2013A610171), Public Science and Technology Research Funds Projects of Ocean (No. 201305013), Key Project in the Educational Office of Fujian Province (No. JA13291), Ningbo Discipline Construction Project Financing (szx11074), and the National Natural Science Foundations (No. 11347173, No. 31201284 and No. 31302192).

References

1. J. Koornneef, P. van Breevoort, C. Hamelinck, C. Hendriks, M. Hoogwijk, K. Koop, M. Koper, T. Dixon and A. Camps, *Int. J. Greenh. Gas Con.*, 11 (2012) 117.
2. S. Mahammadunnisa, E. L. Reddy, D. Ray, C. Subrahmanyam and J. C. Whitehead, *Int. J. Greenh. Gas Con.*, 16 (2013) 361.
3. J. Ma, N. Sun, X. Zhang, N. Zhao, F. Xiao, W. Wei and Y. Sun, *Catal. Today*, 148 (2009) 221.
4. T. Danciu, E. J. Beckman, D. Hancu, R. N. Cochran, R. Grey, D. M. Hajnik and J. Jewson, *Angew. Chem. Int. Ed.*, 42 (2003) 1140.
5. E. E. Bensen, C. P. Kubiak, A. J. Sathrum and J. M. Smieja, *Chem. Soc. Rev.*, 38 (2009) 89.
6. H. Takahashi, L. H. Liu, Y. Yashiro, K. Loku, G. Bignall and N. Yamasaki, *J. Mater. Sci.*, 41 (2006) 1585.
7. H. Yang, Z. Xu, M. Fan, R. Gupta, R. B. Slimane, A. E. Bland and I. Wright, *J. Environ. Sci.*, 20 (2008) 14.
8. S. C. Roy, O. K. Varghese, M. Paulose and C. A. Grimes, *ACS Nano*, 4 (2010) 1259.
9. G. A. Olah, A. Goeppert and G. K. S. Prakash, *J. Org. Chem.*, 74 (2009) 487.
10. C. Costentin, M. Robert and J. M. Savéant, *Chem. Soc. Rev.*, 42 (2013) 2423.
11. A. O. Isenberg, *Solid State Ionics*, 3-4 (1981) 431.
12. A. O. Isenberg, NASA Research Center, *NASA Rreport CR-185612*, 1989.
13. K. R. Sridhar, *J. Br. Interplanet.*, 49 (1996) 435.
14. S. H. Jesen, P. H. Larsen and M. Mogensen, *Int. J. Hydrogen Energy*, 32 (2007) 3253.
15. S. D. Ebbesen and M. Mogensen, *J. Power Sources*, 193 (2009) 349.
16. A. G. Imenes, and D. R. Mills, *Sol. Energy Mater. Sol. Cells*, 84 (2004) 19.
17. D. Barlev, R. Vidu and P. Stroeve, *Sol. Energy Mater. Sol. Cells*, 95 (2011) 2703.
18. Energy efficiency: Texas' newest energy resource. *Solar Energy* [chapter 3], http://www.seco.cpa.state.tx.us/publications/renewenergy/solarenergy.php, 2013-09-27.
19. S. A. Kalogirou, *Prog. Energy Combust. Sci.*, 30 (2004) 231.

20. M. Ni, M. K. H. Leung and D. Y. C. Leung, *Int. J. Hydrogen Energy*, 32 (2007) 4648.
21. Y. Shin, W. Park, J. Chang and J. Park, *Int. J. Hydrogen Energy*, 32 (2007) 1486.
22. H. Zhang, G. Lin and J. Chen, *Int. J. Hydrogen Energy*, 35 (2010) 10851.
23. H. Zhang, J. Wang, S. Su and J. Chen, *Int. J. Hydrogen Energy*, 38 (2013) 9609.
24. M. Ni, *Chem. Eng. J.*, 164 (2010) 246.
25. M. Ni, *J. Power Sources*, 202 (2012) 209.
26. J. Wishart, Z. Dong and M. Secanell, *J. Power Sources*, 161 (2006) 1041.
27. T. Springer, S. Zawodzinksi and S. Gottesfeld, *J. Electrochem. Soc*., 138 (1991) 2334.
28. M. A. Rosen, *Int. J. Hydrogen Energy*, 20 (1995) 547.
29. M. A. Rosen, Exergy as a tool for sustainability. *3rd IASME/WSEAS Int. Conf. on Energy & Environment*, University of Cambridge, UK, Febriary 23-25, 2008.
30. S. K. Tyagi, S. W. Wang, M. K. Singhal, S. C. Kaushik and S. R. Park, *Int. J. Thermal. Sci.*, 46 (2007) 1304.
31. A. Joshi, I. Dincer and B. V. Reddy, *Int. J. Low-Carbon Technol.*, 6 (2011) 64.
32. A. S. Joshi and A. Tiwari, *Renew. Energy*, 32 (2007) 2223.
33. Y. Morita, T. Fujisawa and T. Tani, *Electric. Eng. Japan*, 133 (2000) 43.
34. L. Wu, G. Lin and J. Chen, *Renew. Energy*, 35 (2010) 95.
35. C. F. Mhilu, *ISRN Chem. Eng.*, 437186 (2012) 1.
36. P. H. Li, P. H. Wang and A. T. Huang, *China Steel Technical Report*, 22 (2009) 63.
37. M. Ni, M. K. H. Leung and D. Y. C. Leung, *Int. J. Hydrogen Energy*, 32 (2007) 2305.
38. T. A. H. Ratlamwala, M. A. Gadalla and I. Dincer, *Int. J. Hydrogen Energy*, 36 (2011) 11282.
39. Y. Vorobiev, J. González-Hernández, P. Vorobiev and L. Bulat, *Solar Energy*, 80 (2006) 170.

© 2014 by ESG (www.electrochemsci.org)